Analytica Chimica Acta 1080 (2019) 206–214

Contents lists available at ScienceDirect

Analytica Chimica Acta

journal homepage: www.elsevier.com/locate/aca

Fluorescence hydrogel array based on interfacial cation exchange amplification for highly sensitive microRNA detection

Lina Wu [a], Yingfei Wang [a], Rong He [a], Yue Zhang [a], Yuling He [a], Chao Wang [b], Zhenda Lu [b], Ying Liu [a, *], Huangxian Ju [a]

[a] State Key Laboratory of Analytical Chemistry for Life Science, School of Chemistry and Chemical Engineering, Nanjing University, Nanjing, 210023, PR China
[b] College of Engineering and Applied Science, Nanjing University, Nanjing, 210023, PR China

HIGHLIGHTS

- A fluorescence polyethylene glycol hydrogel array is designed for miRNA detection with limit of detection down to 0.835 fM.
- Hybridization chain reaction (HCR) is performed in hydrogel framework upon target miRNA initiation.
- Fluorescence signal amplification is achieved via interfacial cation exchange in aqueous like environment of hydrogel.
- Direct detections of miRNA-21 were achieved from lysate of 10 equivalent cells and clinical serum samples.

GRAPHICAL ABSTRACT

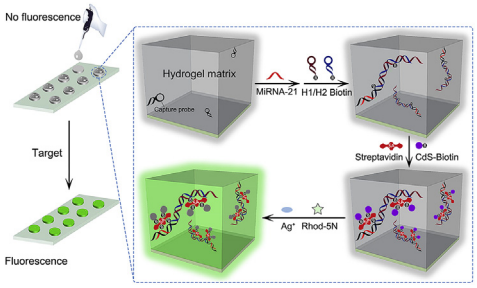

ARTICLE INFO

Article history:
Received 9 May 2019
Received in revised form
9 July 2019
Accepted 11 July 2019
Available online 13 July 2019

Keywords:
PEG hydrogel array
MicroRNA detection
Hybridization chain reaction
Cation exchange fluorescence amplification

ABSTRACT

Despite the great success of fluorescence sensing array application in bioanalysis, the photo-quenching problem accompanied with high surface fluorophore density has become the bottleneck for its further sensitivity improvement. Herein, a fluorescence polyethylene glycol (PEG) hydrogel array was developed for highly sensitive microRNA detection based on interfacial cation exchange amplification coupled with DNA hybridization chain reaction (HCR). The carboxylate PEG hydrogel array was fabricated on glass slide via photo polymerization and modified with miRNA capture probe, target miRNA binding triggered HCR in hydrogel with biotin labelled DNA probes to generate numerous DNA polymer chains where biotinylated CdS QDs were subsequently conjugated with a streptavidin bridge. Interfacial cation exchange amplification was triggered in hydrogel upon the introduction of Ag^{+} and Rhod-5N, and abundant Cd^{2+} was released from CdS to bind with Rhod-5N for substantial fluorescence enhancement. The aqueous-like environment of hydrogel eliminated the fluorescence quenching and simplified experiment process by performing cation exchange reaction at interface with direct result. The linear range for model target miRNA-21 was 1 fM to 500 pM with a detection limit of 0.835 fM. Taking advantage of the non-fouling property of PEG hydrogel, direct quantification of miRNA-21 was achieved from crude cancer cell lysates with a detection limit down to 10 equivalent cells. The expressions of circulating miRNA-21 in clinical serum samples were also assessed with comparable results from RT-PCR. The developed hydrogel

* Corresponding author.
E-mail address: yingliu@nju.edu.cn (Y. Liu).

https://doi.org/10.1016/j.aca.2019.07.024

array provides a universal platform for highly sensitive fluorescence sensing, and would benefit clinical non-invasive disease diagnosis.

1. Introduction

MicroRNAs (miRNAs) are endogenous, evolutionally conserved, noncoding single-stranded RNAs [1], which play crucial role in regulating many disease processes [2], and have emerged as significant disease biomarkers due to their aberrant expressions in various pathological status [3,4]. Therefore, in vitro miRNAs detection could signify the early onset of disease [5] and evaluate therapeutic effect [6].

Due to their short length, low abundance and high similarity among homogeneous sequence [7], miRNAs detection is challenging. Gold standard methods such as Northern blotting [8] and quantitative reverse-transcriptase polymerase chain reaction [9] all require tedious experiment procedures and have limitations either in detection sensitivity [10] or false positive signal [11]. The use of planar substrate based devices for biosensing is a promising approach [12] for clinical diagnosis due to its portability, flexibility, and straightforward operations [13,14]. By coupling with fluorescence readout, recent innovations in optical biochip devices have enabled new technological breakthroughs due to the emerging of organic dyes and fast advancement in optical imaging [12,15–17]. However, the bottleneck for the further sensitivity improvement of fluorescence biochip is the photo-quenching accompanied with high fluorophore density on surface [18,19], and the limit of detection for fluorescence chip based biosensing could hardly get below pM, especially in complex biological environments [20].

Cation exchange [21,22] is a classical ionic nanocrystal synthesis approach in which the cations composing an ionic solid can be exchanged with different cations in facile reaction condition with rapid rate due to the large surface area and small volume of ionic solid. Cation exchange-based fluorescence amplification strategies that use Ag^+ to trigger abundant cations release from semiconductor nanocrystal and subsequently bind to metal responsive fluorophores for much higher quantum yields [18,23–26]. Since the fluorophores are present in detection solutions instead of crowdedly immobilized on planar substrates, photo-quenching is no longer a problem [18]. Each cation composing the nanocrystal contributes to fluorescence generation therefore results in very high detection sensitivity in biosensing [18,23,25–27] and imaging [28]. However, the cation exchange amplification reaction only proceeds in a homogeneous solution, therefore separation and collection of exchanged cations [23,26,29,30] are required before fluorescence measurement, which complicates operation and limits its application in biochip based device. 96-well plates have been applied to locate cation exchange in an array format [31], but both the dilution of exchanged cations in each well with relatively large loading volume and the inefficiency for semiconductor nanocrystal capture in well plates impaired the assay sensitivity.

Unlike planar substrate based biosensing platform, the three-dimensional (3D) hydrogel provides an aqueous reaction environment with solution-like reaction kinetics [32,33], as well as increases the loading capacity of probe molecules and resists nonspecific adsorption [34], therefore has been applied as chip matrix in biosensing [35]. Taking advantages of the polyethylene glycol (PEG) hydrogel array, here we first performed interfacial cation exchange amplification in a biochip manner, which highly improved the signal intensity of fluorescence biochip and achieved convenient miRNA detection from crude cell lysates and patients' serums with impressive sensitivity and selectivity. As shown in Scheme 1, the carboxylate PEG hydrogel array was first fabricated on glass substrate via photo initiated polymerization of PEG-DA and Acryl-PEG-COOH with a photomask, and functionalized with miRNA capture probe. As a promising biomarker for diagnosis and prognosis [36,37], miRNA-21 was chosen as the model target, whose binding initiated hybridization chain reaction (HCR) in PEG hydrogel with the addition of biotin labelled hairpin DNA strands (H1-biotin and H2-biotin). The resulting long DNA strands in hydrogel provided abundant positions for the subsequent binding of biotinylated CdS QDs (CdS-biotin) in a biotin-streptavidin-biotin sandwich format. The hydrogel structure with micrometer sized pores allowed the free diffusions of DNA strands and CdS-biotin, as well as guaranteed high yield of DNA HCR strands and high binding efficiency of CdS-biotin. The interfacial cation exchange reaction was then performed in PEG hydrogel matrix instantaneously upon the introduction of Ag^+ and Rhodamine 5 N (Rhod-5N) dye mixture solution, which formed Ag_2S and released thousands of Cd^{2+} to coordinate with Rhod-5N and generated strong fluorescence for the whole PEG hydrogel matrix. The small size of patterned hydrogel matrix was capable of holding detection solution as low as 10 μL, which not only provided a solution-like environment to facilitate cation exchange reaction, but also concentrated the exchanged Cd^{2+} and Rhod-5N to result higher fluorescence. The fluorescence intensity of the hydrogel matrix demonstrated a linear relationship versus miRNA-21 from 1 fM to 500 pM with a limit of detection as 0.835 fM, much more sensitive than most substrate based fluorescence sensing approaches. Direct quantifications of low abundance miRNA from crude cell lysates and patients' serums were achieved due to the superiority of nonfouling PEG. By diluting the lysate of HepG-2 cells, the proposed method can detect endogenous miRNA-21 down to 10 equivalent cells. In addition, analysis of clinical samples showed a satisfactory result in distinguishing serums of gastric cancer patients and healthy controls. We anticipate the presented fluorescence PEG hydrogel would allow rapid and reliable clinical profiling of miRNAs, and potentially contribute to non-invasive disease diagnosis.

2. Materials and methods

2.1. Reagents

3-Acryloxypropyltrichlorosilane was purchased from Gelest, Inc. (Morrisville, PA). Polyethylene glycol diacrylate (PEG-DA, MW 700) and 2-hydroxy-2-methyl-propiophenone (photoinitiator) were purchased from Sigma-Aldrich (St. Louis, MO). Acrylic polyethylene glycol carboxyl (Acryl-PEG-COOH, MW 3400) and polyethylene glycol diacrylate (PEG-DA, MW 3400) were purchased from ToYong Biotech. Inc. (Shanghai, China). 1-ethyl-3-(3-(dimethylamino)propyl) carbodiimide hydrochloride (EDC), N-hydroxysuccinimide (NHS), and mercaptopropionic acid (MPA, 99%) were obtained from Aladdin Reagent Co., Ltd. (Shanghai, China). Cadmium chloride ($CdCl_2 \cdot 2.5H_2O$) was purchased from Alfa Aesar (Shanghai, China). EZ-Link Amine-PEG_2-Biotin, Streptavidin-Cy3 (SA-Cy3), and Lipofectamine™ 2000 (Lipo-2000) transfection reagent were purchased from Thermo Fisher Scientific Inc. (Rockford, IL). Rhodamine

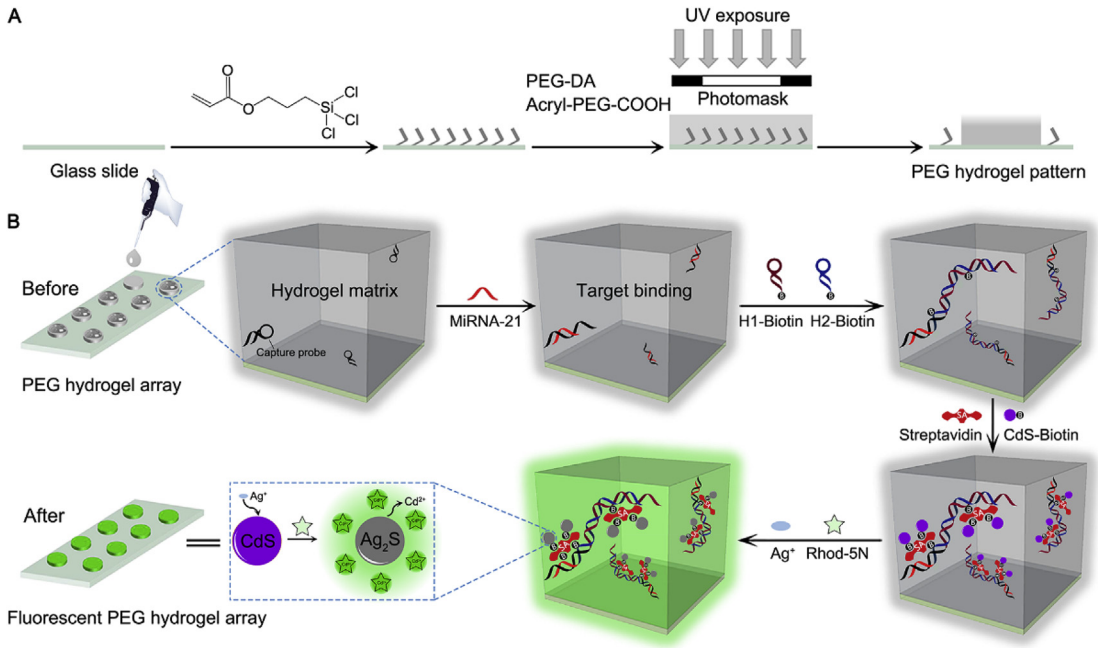

Scheme 1. Schematic illustrations of (A) carboxylate PEG hydrogel array fabrication via photo initiated radical polymerization and (B) interfacial cation exchange fluorescence amplification in PEG hydrogel array for miRNA detection.

5 N (Rhod-5N) was purchased from AAT Bioquest Inc. (Sunnyvale, CA). DEPC (Diethy pyrocarbonate) treated water was used in the throughout process of miRNA operation. The synthetic miRNAs were obtained from GenePharma Co., Ltd. (Shanghai, China), and all of the DNA oligonucleotides were synthesized and purified by Sangon Biotech Co., Ltd. (Shanghai, China) with sequences listed in the following (See Table 1).

2.2. Apparatus

The patterned PEG hydrogel array was fabricated using XC210 UVLED system (Aventk, China), and scanned with GenePix 4100A Microarray Scanner (Molecular Devices, U.S.A.) with corresponding fluorescence intensities analyzed by GenePix Pro 7 Software. The static contact angles were measured with a contact angle system (OCA30, Dataphysic Instruments GmbH, Germany). SEM images were obtained by Quattro environmental scanning electron microscope (FEI Company, U.S.A.) at 10 kV. TEM images were acquired by Tecnai G2 F20 X-TWIN Transmission electron microscope (FEI Company, U.S.A.). Absorption spectra were recorded from UV-3600 UV–vis–NIR spectrophotometer (Shimadzu, Japan) and 6700 Fourier transform infrared spectrophotometer (Nicolet, U.S.A.). Fluorescence spectra were collected with FluoroMax-4 Spectrofluorometer (HORIBA Scientific, Japan). The gel electrophoresis was performed on PowerPac™ Basic electrophoresis analyzer (Bio-Rad, U.S.A.) and imaged on Biorad ChemiDoc XRS facility (Bio-Rad, U.S.A.). Numbers of cells were determined using Countess® II FL Automated Cell Counter (Thermo Fisher Scientific, U.S.A.).

2.3. Fabrication of carboxylate PEG hydrogel array

Glass substrates were cleaned by sonicating in acetone, ethanol and deionized (DI) water for 2 min respectively and dried under N_2. After treated with a PDC-MG plasma cleaning machine for 15 min to activate the surface hydroxyl groups, the glass substrates were incubated in 40 mL toluene solution containing 20 μL 3-acryloxypropyltrichlorosilane for 1 h under N_2 atmosphere at room temperature for surface silanization. After thoroughly rinsed with fresh toluene and copious DI water, the glass slides were dried under N_2 and cured in an oven for 3 h at 100 °C [38].

7.5% (v/v) PEG-DA (MW 700), 22.5% (v/v) of 20 mM PEG-DA (MW 3400) aqueous solution, 40% (v/v) PEG (MW 200), 15% (v/v) of 20 mM Acryl-PEG-COOH aqueous solution, and 10% (v/v) of 655 mM 2-hydroxy-2-methyl-propiophenone (photoinitiator) ethanol solution were mixed in DI water and pipetted onto the

Table 1
Synthetic oligonucleotide sequences.

Name	Sequence (5′ to 3′)
Capture probe	ATCAGACTGATGTTGACAAAGTTCAACATCAGTCTGATAAGCTA-NH_2
H1-biotin	ATCAGACTGATGTTGACAAAGTTCAACATCAGTCTGATAAGCTA-biotin
H2-biotin	biotin-ACTTTGTCAACATCAGTCTGATTAGCTTATCAGACTGATGTTGA
Self-quenched H1	ATCAGACTG/iBHQ2dT/ATGTTGACAAAGTTCAACATC/iCy3dT/AGTCTGATAAGCTA
MiRNA-21	UAG CUU AUC AGA CUG AUG UUG A
MiRNA-141	UAA CAC UGU CUG GUA AAG AUG G
MiRNA-199a	ACA GUA GUC UGC ACA UUG GUU A
1-mismatched	UAG CUU AUC AGA CC̲G AUG UUG A
3-mismatched	UAG CU̲A AUC AGA CC̲G AUG U̲AG A
Inhibitor	UCA AC̲A UCA GUC U̲GA UAA G̲CU A

silanized glass substrate, a cover slip was subsequently covered on the precursor solution to create a uniform fluid layer. The glass substrate was then aligned with a photomask and exposed under 365 nm UV light with 80 mW cm^{-2} for 1.5 s [39]. After scrupulously rinsed with DI water to remove unpolymerized precursor, the prepared carboxylate PEG hydrogel array was kept in DI water or a highly humid environment until use.

2.4. Synthesis of CdS-biotin

92 mg $CdCl_2 \cdot 2.5H_2O$ was dissolved in 20 mL ultrapure water, and transferred into a clean three-necked flask with the subsequent dropwise addition of 86 μL MPA under vigorous stirring. After adjusted the pH of the mixture solution to 10 with 1 M NaOH, 30 mg thioacetamide was dissolved in 20 mL ultrapure water and slowly dropped into the mixture solution with 30 min stirring at room temperature and 10 h reflux at 80 °C [40]. The obtained MPA-capped CdS quantum dot (CdS) was washed with ethanol twice via centrifugation (14000 rpm, 10 min every time), and re-dispersed in pure water kept at 4 °C.

After activating CdS surface carboxyl groups with 0.12 M EDC and NHS in 0.1 M MES buffer (pH 5.5), it was reacted with 50 mM amine-PEG_2-biotin aqueous solution for 5 h. After washed twice with pure water, the as-obtained biotinylated CdS (CdS-biotin) was dissolved in water and kept at 4 °C until use.

2.5. Feasibility analysis

HCR in homogeneous solution was validated by PAGE and fluorescence spectroscopy. For PAGE, 10% native polyacrylamide gel and loading sample including 7 μL DNA sample, 1.5 μL 6 × loading buffer, and 1.5 μL UltraPowerTM dye were respectively prepared. The gel electrophoresis was run at 100 V for 70 min in 1 × TBE buffer. Cy3 and BHQ2 labelled self-quenched H1 and H2 were used for fluorescence characterization. After incubating self-quenched H1 and H2 with miRNA-21 at 37 °C for 2 h, the mixture solution was measured by fluorescence spectrometer, using the excitation wavelength of 532 nm with a slit width of 2 nm. HCR in the hydrogel was validated by incubating self-quenched H1 and H2 with same concentration miRNA-21 in the PEG hydrogel pattern with fluorescence quantification using the microarray scanner with the excitation channel of 532 nm.

Prior to interfacial cation exchange reaction of CdS QDs, the feasibility was validated in homogeneous solution. By mixing Ag^+ and Rhod-5N with CdS dispersed solution, the fluorescence of the reaction solution was measured by fluorescence spectrometer with excitation wavelength of 530 nm and a slit width of 2 nm. 10 μM Cd^{2+}, Pb^{2+}, Zn^{2+}, Ca^{2+}, Mg^{2+}, and Cu^{2+} were mixed with Rhod-5N to demonstrate the reaction selectivity of cation exchange reaction in homogeneous solution.

2.6. MiRNA detection in PEG hydrogel array with interfacial cation exchange

The carboxylate PEG hydrogel array was activated with 10 μL 0.4 M EDC and 0.1 M NHS in 25 mM MES buffer (pH 5.5), and incubated with 0.5 μM capture probe in 1 × SPSC buffer (0.75 M NaCl and 50 mM Na_2HPO_4, pH 7.4) overnight at ambient environment. MiRNA detection experiment was conducted in a humid box. The capture probe immobilized PEG hydrogel pattern was incubated with target miRNA-21 at desired concentration for 1 h at 37 °C, with the subsequent addition of 1:1 mixture of H1-biotin and H2-biotin (1 μM) and 2 h incubation at 37 °C to allow the hybridization chain reaction (HCR). After removing the residual reactants with PBS washing, the PEG hydrogel pattern was continuously incubated with 0.01 mg ml^{-1} streptavidin for 1 h, and 10 μM CdS-biotin for 1 h at room temperature.

After thoroughly washing with PBS containing 0.05% Tween 20, the CdS-biotin loaded PEG hydrogel pattern was incubated with a mixture solution of 500 μM Ag^+ and 2 μM Rhod-5N in 0.1 M KAc buffer (pH 7.4) with a total volume of 2 μL for 10 min to allow the interfacial cation exchange amplification reaction. The PEG hydrogel array was subsequently scanned with a microarray scanner for fluorescence intensity measurement.

3. Results and discussion

3.1. Fabrication of carboxylate PEG hydrogel array and immobilization of DNA capture probe

The glass substrate was modified with acrylate group through silanization, coated with precursor mixture of PEG-DA and Acryl-PEG-COOH, exposed under UV irradiation with a photomask for the generation of a 8 × 3 carboxylate PEG hydrogel array with 5 mm in diameter for each hydrogel pattern (Fig. 1A). The contact angle of glass substrate increased from ~29° to ~55° after silanizaiton, and decreased to ~17° after the conjugation of hydrophilic PEG hydrogel, which corresponded well with literature reported values of hydrogel (Fig. 1A) [41]. FT-IR spectrum of carboxylate PEG hydrogel demonstrated main PEG characteristic peaks at 3400 cm^{-1} for −OH, 2860 cm^{-1} for $-CH_2$, 1735 cm^{-1} for −C═O, 1247 cm^{-1} for -C-O, 1101 cm^{-1} for C−O−C stretching vibrations, and at 948 cm^{-1} for

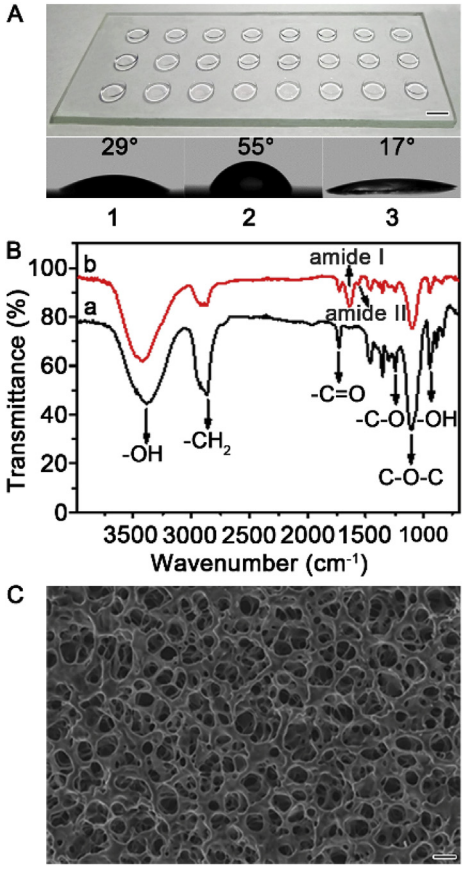

Fig. 1. Characterization of PEG hydrogel array. (A) Photograph of carboxylate hydrogel array patterned on the silanized glass substrate (scale bar: 5 mm) and water droplets on glass (1), silanized glass substrate (2) and carboxylate PEG hydrogel pattern (3). (B) FT-IR spectra of carboxylate PEG hydrogel before (a) and after (b) DNA capture probe immobilization. (C) SEM image of carboxylate PEG hydrogel pattern (scale bar: 10 μm).

–OH deformation vibration (Fig. 1B, line a) [42]. Since the pore size of hydrogel network is dependent on the molecular weight (MW) of PEG-DA [41], PEG-DAs with different MW were used to generate hydrogel with appropriate pore size for HCR. SEM characterization of carboxylate PEG hydrogel demonstrated inter-connected porous microstructure with the pore size of about 10 μm (Fig. 1C), which allowed the free diffusions of subsequent reactants such as DNA probes and CdS-biotin, and guaranteed the reaction efficiency of HCR in PEG hydrogel.

The DNA capture probe with amine terminus was immobilized into carboxylate PEG hydrogel via amidation, and demonstrated characteristic peaks for amide I and II bands at 1635 cm^{-1} for C=O and 1567 cm^{-1} for C–N stretching vibration respectively in FT-IR spectrum [42,43], which was accompanied by the decrease of carboxyl characteristic peak at 1735 cm^{-1} (Fig. 1B, line b), confirming the covalent conjugation of capture probe in carboxylate PEG hydrogel. To further verify the loading of DNA capture probe in PEG hydrogel, JOE dye labelled capture probe with amine terminus was incubated with carboxylate PEG hydrogel, which showed strong fluorescence (Fig. S1). Due to its nonfouling property, bare PEG hydrogel in the absence of Acryl-PEG-COOH showed little fluorescence after incubated with the same JOE dye labelled capture probe (Fig. S1).

3.2. Synthesis of CdS-biotin and verification of cation exchange fluorescence amplification in homogeneous solution

The CdS was synthesized according to a literature reported approach with MPA as surface stabilizer [40] and demonstrated average size of 3 nm in diameter (Fig. 2A) with absorption peak at 427 nm in UV–vis spectrum and maximum emission peak at 650 nm in photoluminescence (PL) spectrum (Fig. 2B). Amine-PEG_2-biotin was subsequently conjugated to CdS via amidation, and increased its hydrodynamic diameter from 4 ± 0.3 nm (Fig. S2A) to 7 ± 0.5 nm (Fig. S2B) from DLS measurements. The zeta potential for CdS was −17 mV from the surface carboxyl groups, which was increased to −12 mV for CdS-biotin due to the consumption of surface carboxyl groups (Fig. S2D). To further confirm the functionalization of biotin on CdS surface, 0.01 mg ml^{-1} streptavidin

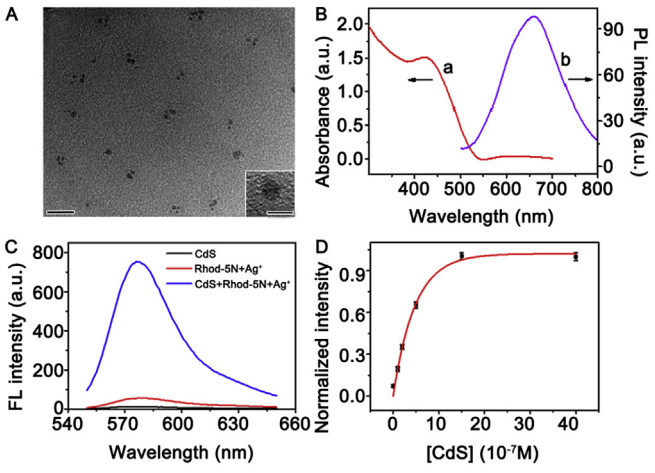

Fig. 2. Characterization of CdS and verification of cation exchange reaction in solution. (A) TEM images of CdS (scale bar: 25 nm). Insert shows the enlarged view of single CdS (scale bar: 5 nm). (B) UV–vis (a) and PL (λ_{ex}: 450 nm) (b) spectra of CdS dispersed in water. (C) Fluorescence spectra of CdS, Rhod-5N before (Ag^++Rhod-5N) and after cation exchange reaction (CdS + Ag^++Rhod-5N). The concentration of CdS, Rhod-5N and Ag^+ were 1.5 μM, 2 μM and 500 μM respectively. (D) Normalized fluorescence intensity of Rhod-5N after cation exchange with CdS of different concentrations. Error bars are standard deviation obtained from three parallel measurements.

was added into the CdS-biotin dispersed solution to trigger the aggregation of CdS-biotin, and the hydrodynamic diameter of assembled CdS nanocluster substantially increased to 142 ± 0.5 nm (Fig. S2C) with the zeta potential decreased to −19 mV due to the negative charge of streptavidin in pH 7.0 reaction solution (Fig. S2D).

The solution based cation exchange fluorescence amplification was triggered by mixing 500 μM Ag^+ and 2 μM Rhod-5N with CdS dispersed solution, the abundant Cd^{2+} released from CdS bound to Rhod-5N and immediately generated strong fluorescence under an excitation wavelength of 530 nm (Fig. 2C). The fluorescence intensity of the maximum emission peak at 576 nm was enhanced ~14 folds compared with that of Rhod-5N and Ag^+ mixture in the absence of CdS (Fig. 2C), and the fluorescence emission from CdS was negligible under 530 nm excitation (Fig. 2C). The cation exchange fluorescence intensity also demonstrated a linear increase with the increment of CdS concentration (taking into account the CdS as an ideal sphere with the bulk density of 4.82 g cm^{-3}), and saturated at about 1.5 μM (Fig. 2D), which confirmed the feasibility of cation exchange fluorescence amplification in quantitative detection. To demonstrate reaction selectivity of Rhod-5N to Cd^{2+}, various metal ions with the same concentration of Cd^{2+} were also mixed with Rhod-5N. Except Pb^{2+} demonstrated 23% fluorescence response and Zn^{2+} demonstrated 14% in contrast to Cd^{2+}, the rest of metal ions all showed negligible fluorescence intensities (Fig. S3), indicating the good selectivity of Rhod-5N to Cd^{2+} over most of interfering cations.

3.3. Feasibility of HCR in PEG hydrogel

MiRNA-21, which was overexpressed in various human cancers and has been identified as an universal biomarker [44], was chosen as the model detection target, and the feasibility of target miRNA-21 triggered HCR was first verified in homogeneous solution with free hairpin DNA strands H1 and H2 via polyacrylamide gel electrophoresis (PAGE) analysis (Fig. 3A). After incubating miRNA-21 with the mixture of H1 and H2, the bands representing H1 and H2 disappeared, while a new ladder shaped band appeared, indicating the successful proceeding of HCR in homogeneous solution. The molecular mass of DNA strand was increased with the decreased concentration of miRNA-21 due to the increased hybridization number of H1 and H2 in HCR product for lower amount trigger, which was in accordance with previous report [45]. Fluorescence spectroscopy was also applied to further confirm HCR in homogeneous solution. Self-quenched H1 was prepared by labelling both fluorescent dye Cy3 and its quencher BHQ2 to H1 probe with close distance to each other in a hairpin structure, and the 1:1 mixture of self-quenched H1 and H2 only demonstrated weak fluorescence (Fig. S4, black line). On the contrast, fluorescence at 580 nm was enhanced about 7 folds compared with the signal from background upon the introduction of 100 nM miRNA-21 due to the unfolding of self-quenched H1 and the assembly of DNA strands (Fig. S4, red line). Incubating self-quenched H1 and H2 1:1 mixture solution with the same concentration of control miRNA of scrambled sequence barely showed fluorescence signal increase compared with background (Fig. S4, blue line), demonstrating the high selectivity of miRNA-21 triggered HCR.

To verify the feasibility of HCR in PEG hydrogel, 100 nM miRNA-21 was incubated with capture probe loaded carboxylate PEG hydrogel with subsequent addition of 1:1 mixture of self-quenched H1 and H2, which showed obvious fluorescence in the carboxylate PEG hydrogel pattern (Fig. 3B, miRNA-21(+)). The fluorescence intensity was about 6.9 folds compared with that of the control experiment for incubating 1:1 mixture of self-quenched H1 and H2 with capture probe loaded carboxylate PEG hydrogel in the absence

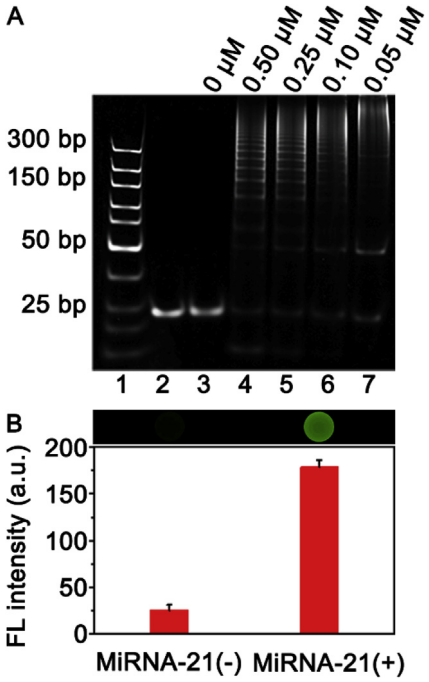

Fig. 3. Verification of HCR in solution and PEG hydrogel. (A) 10% PAGE analysis images. Lanes 1, 300-bp DNA ladder markers; lane 2, 1.0 μM H1; lanes 3–7, 1.0 μM mixture of H1 and H2 in response to various concentrations of miRNA-21 (0, 0.50, 0.25, 0.10 and 0.05 μM). (B) Comparison of fluorescence intensities for 1 μM self-quenched H1 and H2 1:1 mixture solution in the absence and presence of 100 nM miRNA-21. (Insert: corresponding fluorescence images). Error bars are standard deviation obtained from three parallel measurements.

of miRNA-21 (Fig. 3B, miRNA-21(−)), and the fluorescence enhancement factor was similar to that of HCR reaction in homogeneous solution, which indicated the little interference of PEG hydrogel framework on HCR reaction efficiency.

3.4. MiRNA detection in PEG hydrogel with interfacial cation exchange fluorescence amplification

The concentrations of H1/H2 probe, Rhod-5N, and Ag^+ were optimized before preforming interfacial cation exchange reaction, and demonstrated strongest fluorescence intensity with 1 μM H1/H2 probe (Fig. S5), 2 μM Rhod-5N (Fig. S6) and 500 μM Ag^+ (Fig. S7). Various concentrations of miRNA-21 were incubated with the capture probe loaded carboxylate PEG hydrogel patterns respectively, and the 1:1 mixture solution of 1 μM H1-biotin and H2-biotin was added subsequently to trigger HCR in PEG hydrogel. The growth of DNA strands in PEG hydrogel provided abundant binding positions for subsequent CdS-biotin conjugation via a streptavidin bridge. Interfacial cation exchange reaction was directly performed in CdS-biotin conjugated PEG hydrogel by introducing a mixture solution of 500 μM Ag^+ and 2 μM Rhod-5N. Due to the small size and large surface area of CdS-biotin, the cation exchange reaction was performed at very rapid rate, and the abundant released Cd^{2+} bind to Rhod-5N to generate fluorescence with high quantum yield in PEG hydrogel pattern. The fluorescent PEG hydrogel was immediately scanned with the microarray scanner for fluorescence quantification, which increased gradually with miRNA-21 concentration, and demonstrated good reproducibility between patterns (Fig. 4A). By plotting fluorescence intensity of the PEG hydrogel pattern versus the logarithm of miRNA-21 concentration, it demonstrated a linear relationship from 1 fM to 500 pM with a limit of detection (LOD) of 0.835 fM determined by extrapolating the concentration from the signal equal to blank signal plus 3SD of the blank signal (Fig. 4B), which equaled to 8.35 zmol in 10 μL of loading volume for each hydrogel pattern. The LOD of the presented fluorescence hydrogel array was much improved compared with most fluorescence biosensing approaches with signal amplification strategies [46–49]. CdS QDs rather than CdS nanocluster were used in interfacial cation exchange due to their higher binding affinity with DNA strands incorporated in PEG hydrogel and the free diffusions of exchanged cations in PEG hydrogel. Taking into account the total volume of hydrogel pattern was 3.14 mm^3, the densities of DNA strands after HCR in hydrogel pattern were estimated for different miRNA concentrations from 1 fM to 500 pM, which indicated each DNA strand occupied a sphere space with radius from 1 to 80 μm. Considering the common length of DNA cascade reaction product was below micrometer range [50] as well as the rigid structure of DNA strands, here the biotin functionalized DNA strands would have little crosslink upon streptavidin addition and provide sufficient space for subsequent CdS binding. To further demonstrate the superiority of 3D hydrogel platform, interfacial cation exchange reaction was also performed on a planar substrate immobilized with miRNA-21 capture probe. After HCR and cation exchange reaction, the solution from the planar substrate was collected and measured by fluorescence spectrometer, which barely demonstrated fluorescence difference between 1 pM miRNA-21 and blank solution (Fig. S8), indicating a much higher LOD than the interfacial cation exchange reaction preformed in 3D hydrogel.

To demonstrate the superiority of coupling interfacial cation exchange reaction with HCR, HCR amplification was performed alone in PEG hydrogel for miRNA-21 detection, and the result was quantified by conjugating Cy3 labelled streptavidin to biotinylated HCR products, and the lower linear range was achieved as 100 pM (Fig. S9). Cation exchange fluorescence amplification was also performed alone in PEG hydrogel by incubating various concentrations of miRNA-21 captured PEG hydrogel patterns with H2-biotin and subsequently conjugating CdS-biotin via a streptavidin bridge, which extended the lower linear range to 1 pM (Fig. S9). The interfacial cation exchange reaction in DNA strands conjugated PEG hydrogel further extended the lower detection range to 1 fM, which was 5 orders of magnitude lower compared with HCR amplification alone and 3 orders of magnitude lower compared with cation exchange amplification alone (Fig. 4C). The impressive biosensing performance of the presented approach was attributed to the synergetic contribution of HCR in PEG hydrogel with corresponding CdS-biotin accumulation and highly efficient cation exchange fluorescence amplification.

The PEG hydrogel array patterns were also incubated with 1 pM miRNA-199a, miRNA-141, and noncomplementary miRNAs with 3 mismatched bases and 1 mismatched base, and all of the noncomplementary miRNAs barely showed fluorescence intensity difference compared with the background fluorescence in the absence of miRNA-21 (Fig. 4D). The outstanding capability of base mismatch discrimination allows the potential application of PEG hydrogel array in real samples analysis.

3.5. MiRNA detection in crude cell lysates

Due to the outstanding biosensing performance of fluorescence PEG hydrogel array, it was applied to determine the level of endogenous target miRNA-21 in crude cell lysates. The lysates from 10^4 hepatocellular carcinoma cells (HepG-2) were serially diluted and incubated with PEG hydrogel array, which demonstrated decreased fluorescence after cation exchange amplification with the equivalent numbers of HepG-2 cell decrease (Fig. 5A). The LOD was calculated as low as 10 equivalent cells, which was lower than

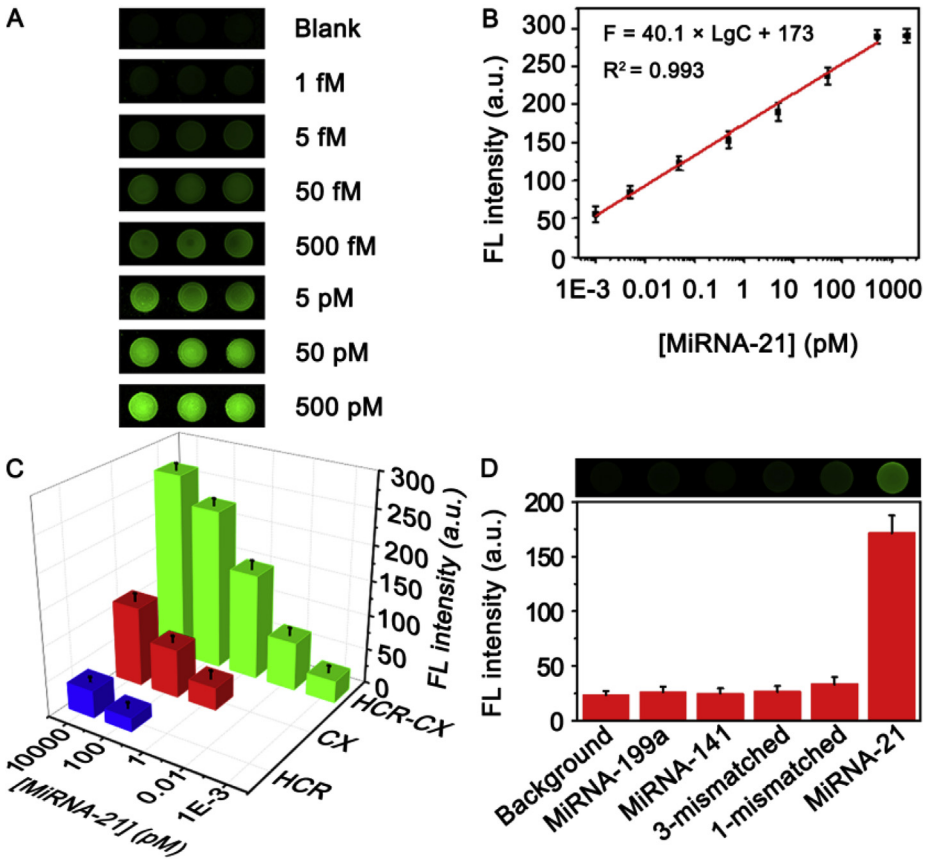

Fig. 4. MiRNA detection with fluorescence PEG hydrogel array based on interfacial cation exchange amplification. (A) Fluorescence images of PEG hydrogel array with various concentrations of miRNA-21 ranging from 1 fM to 500 pM. (B) The linear relationship of fluorescence intensity versus logarithm of miRNA-21 concentration. (C) Comparison of hydrogel patterns fluorescence intensities for HCR amplification (blue columns), cation exchange (CX) amplification (red columns) and HCR-CX combination amplification (green columns) with miRNA-21 concentrations of 1 fM, 10 fM, 1 pM, 100 pM and 10 nM. (D) Selectivity investigation of interfacial cation exchange amplification to 1 pM miRNA-21 and noncomplementary miRNAs. (Insert: corresponding fluorescence images). Error bars are standard deviation obtained from three parallel measurements. (For interpretation of the references to colour in this figure legend, the reader is referred to the Web version of this article.)

literature reported values [51–53], implying the capability of PEG hydrogel array in direct quantifying miRNA from lysates of small number cells.

To further evaluate the reliability of miRNA detection in cell lysates, miRNA-21 mimic and inhibitor were transfected into human cervix carcinoma cells (HeLa) to modulate intracellular miRNA-21 expressions, and the lysates from 2×10^5 treated HeLa cells were incubated with fluorescence PEG hydrogel array for miRNA-21 detection. Meanwhile, RT-PCR was employed to validate the transfection accuracy by means of a miRNA-21 calibration curve with a linear range of 100 fM−1 nM (Fig. S10). Compared with the fluorescence from untreated HeLa cell lysates, miRNA-21 mimic transfected HeLa cell lysates demonstrated stronger fluorescence in PEG hydrogel array, while the miRNA-21 inhibitor transfected HeLa cell lysates showed lower fluorescence (Fig. S11A). The corresponding miRNA-21 expression levels in treated HeLa cells were determined from the calibration curve in Fig. 4B and exhibited as relative expression levels in Fig. 5B, which were coincided well with the results from RT-PCR analysis (Fig. S11B). The lysates from 10^6 cells of different cancer cell lines including HepG-2, HeLa and breast cancer cells (MCF-7) were further analyzed with fluorescence PEG hydrogel array (Fig. S12A), and miRNA-21 concentration from different cell lysates were determined according to the calibration curve in Fig. 4B and convert to the copy number of miRNA-21 per cell, which were in full agreement with those measured by RT-PCR (Fig. 5C, Fig. S12B). The tendency of miRNA-21 expression difference in HepG-2, MCF-7 and HeLa cells were also well corresponded with previously reported measurements [51,54], indicating the high detection accuracy of fluorescence PEG hydrogel array in cell lysates analysis.

3.6. Circulating miRNA detection in serum

With its overexpression in various cancer cells and secreted in exosomes, microvesicles and RNA-binding-proteins, miRNA-21 is also an important circulating miRNA and served as a disease biomarker in non-invasive cancer diagnosis [55,56]. To further explore the application of the fluorescence PEG hydrogel array in clinical sample analysis, it was also applied to detect circulating miRNA-21 from serum samples of gastric cancer patients and healthy donors. The fluorescence intensity from PEG hydrogel pattern incubated with gastric cancer patients' serum sample was obviously higher than that from healthy donors' (Fig. S13A, red columns), confirming the up-regulated expression level of miRNA-21. To verify the assay accuracy, circulating miRNAs were also extracted from gastric cancer patients' and healthy donors' serum samples and incubated with the PEG hydrogel patterns, which demonstrated similar fluorescence intensities as that of serum samples directly incubated hydrogel patterns (Fig. S13A, black columns). The concentrations of miRNA-21 for different serum samples were calculated according to the calibration curve in Fig. 4B, which were well corresponded with the miRNA

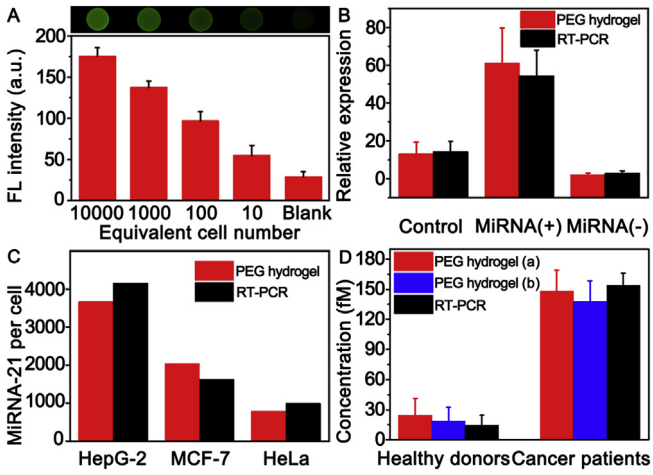

Fig. 5. MiRNA-21 detection from cancer cell lysates and human serums. (A) PEG hydrogel fluorescence intensity according to HepG-2 cell lysates with equivalent cell numbers from 10 to 10^4. (Insert: corresponding fluorescence images). (B) Relative expression levels of miRNA-21 in untreated (control), miRNA-21 mimic (miRNA(+)) and inhibitor treated (miRNA(−)) HeLa cells determined with fluorescence PEG hydrogel and RT-PCR. The expression level of miRNA-21 inhibitor treated HeLa cells was taken as a calibrator (set to 1) to calculate the relative expression levels in untreated and mimic treated HeLa cells. (C) Average miRNA-21 copy number per cell for HepG-2, MCF-7 and HeLa cells determined with fluorescence PEG hydrogel and RT-PCR. (D) Quantification of circulating miRNA-21 in serums of healthy donors and gastric cancer patients with fluorescence PEG hydrogel incubated with serum samples (a), miRNAs extracted from serum samples (b) and RT-PCR. Error bars are standard deviation obtained from three parallel measurements.

quantification results from RT-PCR (Fig. 5D, Fig. S13B) and literature reported values [44,55,57]. The nonfouling property of PEG hydrogel contributed to the direct quantification of circulating miRNA from serum samples, which would hold great potential for non-invasive cancer diagnosis.

4. Conclusions

In summary, we developed a highly sensitive miRNA sensing array based on interfacial cation exchange fluorescence amplification combined with HCR in PEG hydrogel. The impressive biosensing performance with LOD down to 0.835 fM resulted from the abundant CdS loading positions provided by HCR and high quantum yield of cation exchange fluorescence amplification, which was performed in hydrogel environment thus eliminating quenching problem from fluorescent planar substrate. Endogenous miRNA-21 from cell lysates and circulating miRNA-21 from cancer patients and healthy donors were determined, and the results were consistent well with those obtained from RT-PCR. The method provides a universal platform for non-invasive miRNA sensing with high sensitivity, thus has promising potential in clinical diagnosis and therapeutic effect evaluation.

Acknowledgements

We gratefully acknowledge the National Natural Science Foundation of China (21605083, 21635005), Natural Science Foundation of Jiangsu Province (BK20160644), and the National Research Foundation for Thousand Youth Talents Plan of China. State Key Laboratory of Analytical Chemistry for Life Science (5431ZZXM1806), Specially-Appointed Professor Foundation of Jiangsu Province, and Program for Innovative Talents and Entrepreneurs of Jiangsu Province.

Appendix A. Supplementary data

Supplementary data to this article can be found online at https://doi.org/10.1016/j.aca.2019.07.024.

References

[1] L. He, G.J. Hannon, MicroRNAs: small RNAs with a big role in gene regulation, Nat. Rev. Genet. 5 (2004) 522–531.
[2] S. Volinia, G.A. Calin, C.G. Liu, S. Ambs, A. Cimmino, F. Petrocca, R. Visone, M. Iorio, C. Roldo, M. Ferracin, R.L. Prueitt, N. Yanaihara, G. Lanza, A. Scarpa, A. Vecchione, M. Negrini, C.C. Harris, C.M. Croce, A microRNA expression signature of human solid tumors defines cancer gene targets, Proc. Natl. Acad. Sci. U.S.A. 103 (2006) 2257–2261.
[3] C.C. Pritchard, H.H. Cheng, M. Tewari, MicroRNA profiling: approaches and considerations, Nat. Rev. Genet. 13 (2012) 358–369.
[4] H. Dong, J. Lei, L. Ding, Y. Wen, H. Ju, X. Zhang, MicroRNA: function, detection, and bioanalysis, Chem. Rev. 113 (2013) 6207–6233.
[5] N.E. Larkey, C.K. Almlie, V. Tran, M. Egan, S.M. Burrows, Detection of miRNA using a double-strand displacement biosensor with a self-complementary fluorescent reporter, Anal. Chem. 86 (2014) 1853–1863.
[6] X. Tang, R. Deng, Y. Sun, X. Ren, M. Zhou, J. Li, Amplified tandem spinach-based aptamer transcription enables low background miRNA detection, Anal. Chem. 90 (2018) 10001–10008.
[7] D.P. Bartel, MicroRNAs: genomics, biogenesis, mechanism, and function, Cell 116 (2004) 281–297.
[8] E. Berezikov, F. Thuemmler, L.W. van Laake, I. Kondova, R. Bontrop, E. Cuppen, R.H. Plasterk, Diversity of microRNAs in human and chimpanzee brain, Nat. Genet. 38 (2006) 1375–1377.
[9] C. Chen, D.A. Ridzon, A.J. Broomer, Z. Zhou, D.H. Lee, J.T. Nguyen, M. Barbisin, N.L. Xu, V.R. Mahuvakar, M.R. Andersen, K.Q. Lao, K.J. Livak, K.J. Guegler, Real-time quantification of microRNAs by stem-loop RT-PCR, Nucleic Acids Res. 33 (2005) e179.
[10] M. Lagos-Quintana, R. Rauhut, W. Lendeckel, T. Tuschl, Identification of novel genes coding for small expressed RNAs, Science 294 (2001) 853.
[11] E. Varkonyi-Gasic, R. Wu, M. Wood, E.F. Walton, R.P. Hellens, Protocol: a highly sensitive RT-PCR method for detection and quantification of microRNAs, Plant Methods 3 (2007) 12.
[12] X. Hu, Y. Wang, H. Liu, J. Wang, Y. Tan, F. Wang, Q. Yuan, W. Tan, Naked eye detection of multiple tumor-related mRNAs from patients with photonic-crystal micropattern supported dual-modal upconversion bioprobes, Chem. Sci. 8 (2017) 466–472.
[13] S.K. Vashist, E. Lam, S. Hrapovic, K.B. Male, J.H.T. Luong, Immobilization of antibodies and enzymes on 3-aminopropyltriethoxysilane-functionalized bioanalytical platforms for biosensors and diagnostics, Chem. Rev. 114 (2014) 11083–11130.
[14] Y. Bourquin, A. Syed, J. Reboud, L.C. Ranford-Cartwright, M.P. Barrett, J.M. Cooper, Rare-cell enrichment by a rapid, label-free, ultrasonic isopycnic technique for medical diagnostics, Angew. Chem. Int. Ed. 53 (2014) 5587–5590.
[15] J. Rodriguez-Manzano, M.A. Karymov, S. Begolo, D.A. Selck, D.V. Zhukov, E. Jue, R.F. Ismagilov, Reading out single-molecule digital RNA and DNA isothermal amplification in nanoliter volumes with unmodified camera phones, ACS Nano 10 (2016) 3102–3113.
[16] W. Chen, Q. Li, W. Zheng, F. Hu, G. Zhang, Z. Wang, D. Zhang, X. Jiang, Identification of bacteria in water by a fluorescent array, Angew. Chem. Int. Ed. 126 (2014) 13954–13959.
[17] J. Han, H. Cheng, B. Wang, M.S. Braun, X. Fan, M. Bender, W. Huang, C. Domhan, W. Mier, T. Lindner, K. Seehafer, M. Wink, U.H.F. Bunz, A polymer/peptide complex-based sensor array that discriminates bacteria in urine, Angew. Chem. Int. Ed. 56 (2017) 15246–15251.
[18] J. Li, T. Zhang, J. Ge, Y. Yin, W. Zhong, Fluorescence signal amplification by cation exchange in ionic nanocrystals, Angew. Chem. Int. Ed. 48 (2009) 1588–1591.
[19] J. Hou, H. Zhang, Q. Yang, M. Li, Y. Song, L. Jiang, Bio-inspired photonic-crystal microchip for fluorescent ultratrace detection, Angew. Chem. Int. Ed. 53 (2014) 5791–5795.
[20] H. Zhang, Y. Wang, D. Zhao, D. Zeng, J. Xia, A. Aldalbahi, C. Wang, L. San, C. Fan, X. Zuo, X. Mi, Universal fluorescence biosensor platform based on graphene quantum dots and pyrene-functionalized molecular beacons for detection of microRNAs, ACS Appl. Mater. Interfaces 7 (2015) 16152–16156.
[21] D.H. Son, S.M. Hughes, Y. Yin, A. Paul Alivisatos, Cation exchange reactions in ionic nanocrystals, Science 306 (2004) 1009.
[22] J.B. Rivest, P.K. Jain, Cation exchange on the nanoscale: an emerging technique for new material synthesis, device fabrication, and chemical sensing, Chem. Soc. Rev. 42 (2013) 89–96.
[23] J. Yao, K. Flack, L. Ding, W. Zhong, Tagging the rolling circle products with nanocrystal clusters for cascade signal increase in the detection of miRNA, Analyst 138 (2013) 3121–3125.
[24] J. Yao, X. Han, S. Zeng, W. Zhong, Detection of femtomolar proteins by nonfluorescent ZnS nanocrystal clusters, Anal. Chem. 84 (2012) 1645–1652.
[25] J. Yao, S. Schachermeyer, Y. Yin, W. Zhong, Cation exchange in ZnSe nanocrystals for signal amplification in bioassays, Anal. Chem. 83 (2011) 402–408.

[26] J. Li, S. Schachermeyer, Y. Wang, Y. Yin, W. Zhong, Detection of microRNA by fluorescence amplification based on cation-exchange in nanocrystals, Anal. Chem. 81 (2009) 9723–9729.
[27] Z. Sheng, D. Hu, P. Zhang, P. Gong, D. Gao, S. Liu, L. Cai, Cation exchange in aptamer-conjugated CdSe nanoclusters: a novel fluorescence signal amplification for cancer cell detection, Chem. Commun. 48 (2012) 4202–4204.
[28] X. Liu, G.B. Braun, M. Qin, E. Ruoslahti, K.N. Sugahara, In vivo cation exchange in quantum dots for tumor-specific imaging, Nat. Commun. 8 (2017) 343.
[29] E. Han, L. Ding, H. Ju, Highly sensitive fluorescent analysis of dynamic glycan expression on living cells using glyconanoparticles and functionalized quantum dots, Anal. Chem. 83 (2011) 7006–7012.
[30] J. Xu, Q.M. Zhang, D.X. Zhao, Y.R. Liu, P. Chen, G.H. Lu, H.Y. Xie, High sensitive detection method for protein by combining the magnetic separation with cation exchange based signal amplification, Talanta 168 (2017) 91–99.
[31] R. Hu, T. Liu, X.B. Zhang, Y. Yang, T. Chen, C. Wu, Y. Liu, G. Zhu, S. Huan, T. Fu, W. Tan, DLISA : a DNAzyme-based ELISA for protein enzyme-free immunoassay of multiple analytes, Anal. Chem. 87 (2015) 7746–7753.
[32] M.A. Lifson, J.A. Carter, B.L. Miller, Functionalized polymer microgel particles enable customizable production of label-free sensor arrays, Anal. Chem. 87 (2015) 7887–7893.
[33] H. Lee, S.J. Shapiro, S.C. Chapin, P.S. Doyle, Encoded hydrogel microparticles for sensitive and multiplex microRNA detection directly from raw cell lysates, Anal. Chem. 88 (2016) 3075–3081.
[34] G.C. Le Goff, R.L. Srinivas, W.A. Hill, P.S. Doyle, Hydrogel microparticles for biosensing, Eur. Polym. J. 72 (2015) 386–412.
[35] J. Zhou, C. Liao, L. Zhang, Q. Wang, Y. Tian, Molecular hydrogel-stabilized enzyme with facilitated electron transfer for determination of H2O2 released from live cells, Anal. Chem. 86 (2014) 4395–4401.
[36] B. Bo, T. Zhang, Y. Jiang, H. Cui, P. Miao, Triple signal amplification strategy for ultrasensitive determination of miRNA based on duplex specific nuclease and bridge DNA-gold nanoparticles, Anal. Chem. 90 (2018) 2395–2400.
[37] X. Zhang, Z. Yang, Y. Chang, M. Qing, R. Yuan, Y. Chai, Novel 2D-DNA-nanoprobe-mediated enzyme-free-target-recycling amplification for the ultrasensitive electrochemical detection of microRNA, Anal. Chem. 90 (2018) 9538–9544.
[38] Y. Liu, Y. Liu, Z. Matharu, A. Rahimian, A. Revzin, Detecting multiple cell-secreted cytokines from the same aptamer-functionalized electrode, Biosens. Bioelectron. 64 (2015) 43–50.
[39] K.J. Son, D.S. Shin, T. Kwa, Y. Gao, A. Revzin, Micropatterned sensing hydrogels integrated with reconfigurable microfluidics for detecting protease release from cells, Anal. Chem. 85 (2013) 11893–11901.
[40] E. Han, L. Ding, S. Jin, H. Ju, Electrochemiluminescent biosensing of carbohydrate-functionalized CdS nanocomposites for in situ label-free analysis of cell surface carbohydrate, Biosens. Bioelectron. 26 (2011) 2500–2505.
[41] H. Zhang, L. Wang, L. Song, G. Niu, H. Cao, G. Wang, H. Yang, S. Zhu, Controllable properties and microstructure of hydrogels based on crosslinked poly(ethylene glycol) diacrylates with different molecular weights, J. Appl. Polym. Sci. 121 (2011) 531–540.
[42] K.-G. Noh, S.-Y. Park, Biosensor array of interpenetrating polymer network with photonic film templated from reactive cholesteric liquid crystal and enzyme-immobilized hydrogel polymer, Adv. Funct. Mater. 28 (2018) 1707562.
[43] W. Tu, H. Cao, L. Zhang, J. Bao, X. Liu, Z. Dai, Dual signal amplification using gold nanoparticles-enhanced zinc selenide nanoflakes and P19 protein for ultrasensitive photoelectrochemical biosensing of microRNA in cell, Anal. Chem. 88 (2016) 10459–10465.
[44] B. Wang, Q. Zhang, The expression and clinical significance of circulating microRNA-21 in serum of five solid tumors, J. Cancer Res. Clin. Oncol. 138 (2012) 1659–1666.
[45] Z. Ge, M. Lin, P. Wang, H. Pei, J. Yan, J. Shi, Q. Huang, D. He, C. Fan, X. Zuo, Hybridization chain reaction amplification of microRNA detection with a tetrahedral DNA nanostructure-based electrochemical biosensor, Anal. Chem. 86 (2014) 2124–2130.
[46] Y. Xu, H. Wang, C. Luan, F. Fu, B. Chen, H. Liu, Y. Zhao, Porous hydrogel encapsulated photonic barcodes for multiplex microRNA quantification, Adv. Funct. Mater. 28 (2018) 1704458.
[47] S.J. Zhen, X. Xiao, C.H. Li, C.Z. Huang, An enzyme-free DNA circuit-assisted graphene oxide enhanced fluorescence anisotropy assay for microRNA detection with improved sensitivity and selectivity, Anal. Chem. 89 (2017) 8766–8771.
[48] R. Yuan, X. Yu, Y. Zhang, L. Xu, W. Cheng, Z. Tu, S. Ding, Target-triggered DNA nanoassembly on quantum dots and DNAzyme-modulated double quenching for ultrasensitive microRNA biosensing, Biosens. Bioelectron. 92 (2017) 342–348.
[49] T. Wei, D. Du, Z. Wang, W. Zhang, Y. Lin, Z. Dai, Rapid and sensitive detection of microRNA via the capture of fluorescent dyes-loaded albumin nanoparticles around functionalized magnetic beads, Biosens. Bioelectron. 94 (2017) 56–62.
[50] K. Ren, Y. Xu, Y. Liu, M. Yang, H. Ju, A responsive "nano string light" for highly efficient mRNA imaging in living cells via accelerated DNA cascade reaction, ACS Nano 12 (2018) 263–271.
[51] F. Yin, H. Liu, Q. Li, X. Gao, Y. Yin, D. Liu, Trace microRNA quantification by means of plasmon-enhanced hybridization chain reaction, Anal. Chem. 88 (2016) 4600–4604.
[52] S. Su, Y. Wu, D. Zhu, J. Chao, X. Liu, Y. Wan, Y. Su, X. Zuo, C. Fan, L. Wang, On-electrode synthesis of shape-controlled hierarchical flower-like gold nanostructures for efficient interfacial DNA assembly and sensitive electrochemical sensing of microRNA, Small 12 (2016) 3794–3801.
[53] Y. Liao, R. Huang, Z. Ma, Y. Wu, X. Zhou, D. Xing, Target-triggered enzyme-free amplification strategy for sensitive detection of microRNA in tumor cells and tissues, Anal. Chem. 86 (2014) 4596–4604.
[54] S. Tang, Y. Gu, H. Lu, H. Dong, K. Zhang, W. Dai, X. Meng, F. Yang, X. Zhang, Highly-sensitive microRNA detection based on bio-bar-code assay and catalytic hairpin assembly two-stage amplification, Anal. Chim. Acta 1004 (2018) 1–9.
[55] M. Tsujiura, D. Ichikawa, S. Komatsu, A. Shiozaki, H. Takeshita, T. Kosuga, H. Konishi, R. Morimura, K. Deguchi, H. Fujiwara, K. Okamoto, E. Otsuji, Circulating microRNAs in plasma of patients with gastric cancers, Br. J. Canc. 102 (2010) 1174–1179.
[56] X. Chen, Y. Ba, L. Ma, X. Cai, Y. Yin, K. Wang, J. Guo, Y. Zhang, J. Chen, X. Guo, Q. Li, X. Li, W. Wang, Y. Zhang, J. Wang, X. Jiang, Y. Xiang, C. Xu, P. Zheng, J. Zhang, R. Li, H. Zhang, X. Shang, T. Gong, G. Ning, J. Wang, K. Zen, J. Zhang, C.Y. Zhang, Characterization of microRNAs in serum: a novel class of biomarkers for diagnosis of cancer and other diseases, Cell Res. 18 (2008) 997–1006.
[57] H. Schwarzenbach, N. Nishida, G.A. Calin, K. Pantel, Clinical relevance of circulating cell-free microRNAs in cancer, Nat. Rev. Clin. Oncol. 11 (2014) 145–156.